Proceedings of the ASME 2024
International Mechanical Engineering Congress and Exposition
IMECE 2024
November 17-21, 2024, Portland, OR, USA

IMECE2024-145778

NON-SPHERICAL DROPLET DISPERSION IN HOMOGENEOUS ISOTROPIC TURBULENT FLOW

Yushu Lin*, John Palmore Jr.
Department of Mechanical Engineering
University of Washington, Seattle, WA, USA

ABSTRACT

Motivated by the study of spray combustion in aviation gas turbine engines, this work addresses the dispersion of non-spherical droplets in turbulence. The most popular strategy for modeling spray is using the Lagrangian particle tracking (LPT) method, which represents the spray as consisting of discrete collection of spherical particles. One limitation of this approach is that it neglects the importance of droplet deformation on the dynamics of sprays. Several past works have discussed the importance of non-sphericity in modeling real droplets including works conducted by our research group. Some of our past work has demonstrated the importance of the deformation on droplet vaporization, combustion and drag. However, those works have investigated the effect of deformation on droplets in simple configurations such as isolated droplets in uniform flows. The purpose of this work is to investigate the effect of droplet deformation on spray dynamics in a more practical configuration of droplets in turbulent flows. By utilizing an in-house code developed for multiphase flows, this work uses homogeneous isotropic turbulence (HIT) as the framework to investigate how the trajectories of non-spherical particles differ from spherical ones. The temporal Lagrangian autocorrelation of non-spherical droplet velocity is higher than that of spherical droplet, showing a better dispersion of non-spherical droplet. The mean Stokes number shows the dominance of inertia effect of droplets, and a higher mean Stokes number for non-spherical droplets indicates a weaker droplet clustering or preferential concentration.

Keywords: non-spherical droplet, particle dispersion, homogeneous isotropic turbulence

1 INTRODUCTION

The purpose of this work is to investigate the dispersion of non-spherical droplets in turbulence. The dispersion of droplets is important in many engineering applications, for example spray combustion in aviation gas turbine engines. We aim to diminish the gap between theories in literature of spray modeling. One of the most popular strategy for modeling spray is to use the Lagrangian particle tracking method, which represents the spray as a discrete collection of point particles. One limitation of this approach is that it neglects the importance of droplet deformation on the dynamics of sprays. The particles in LPT method are usually treated as spherical particles. Several our past works have already demonstrated the importance of non-sphericity in modeling real droplets. The effect of deformation of droplets on vaporization [1] , combustion [2], and drag [3] have been examined. However, these work have only considered simple configurations of droplets, for example isolated droplets in a uniform inflow. Therefore, in this work, we will extend our previous studies to a more practical configuration to study the effect of droplet deformation on spray dynamics in turbulent flow.

The work will use homogeneous isotropic turbulence (HIT) as the framework to study this phenomenon, and this preliminary investigation will focus on how the trajectories of non-spherical particles differ from spherical ones. HIT was chosen because it is a canonical framework to investigate the turbulent flows in a simplified and well-controlled environment. The ultimate impact of

*linysh@uw.edu

this work will be in understanding the process of fuel mixing and combustion in sprays. Knowledge of the motion of the droplets themselves is key to predicting how mixing will proceed, since the evaporation of droplets is what causes the release of the fuel vapor to mix and combust. In addition, from the environmental perspective, a better understanding of spray will be helpful for people to develop and test non-petroleum based fuels to reduce the pollution and carbon emission in industrial production activities.

This work leverages our research group's in house code for multiphase flows. The gas phase is modeled by using an in-house solver developed by Palmore and Desjardins (2018) for solving high Reynolds number turbulent flows [4]. The droplets are modeled by using a Lagrangian particle tracking solver designed by Capecelatro and Desjardins (2013) to simulate the full range of dilute-to-dense particle laden flows [5]. Droplet deformation is modeled in literature including Ref. [3, 6, 7]. In this work, the Lagrangian particle tracking will be supplemented with a Weber number correlation based method in Ref. [7]. The analysis will compare the dispersion of real droplets to spherical droplets of the same size to measure the effect of deformation. The dispersion of the particles will be measured explicitly by using Taylor's autocorrelation theory [8] and implicitly through measures such as analysis of the particle volume fraction.

2 Configurations

To investigate the dispersion of non-spherical droplets in the HIT flow, we simulate the droplets and flow in a 3D cubic box. Periodic boundary conditions has been applied to all boundaries of the cubic domain. The domain size has a length scale of $L = 0.044$ m in all directions, and a uniform mesh with $N = 256$ in each direction is applied. For schematic purpose, the spacial distribution of droplets in the domain, the velocity magnitude, and the vorticity magnitude of the HIT flow, has been illustrated in Fig.1.

2.1 Parameters

The gas phase has a density of $\rho = 0.790$ kg/m^3 and kinematic viscosity of $\nu = 3.13 \times 10^{-5}$ m^2/s. The turbulence properties are listed in Table.1. In this table, l is the length scale of large eddies in the turbulence, ε is the dissipation rate of the turbulent flow, and u' is the root-mean-square of gas velocity fluctuation, defined as:

$$u' = \sqrt{\left\langle |u - \langle u \rangle|^2 \right\rangle} \tag{1}$$

where $\langle \cdot \rangle$ is the mean operation. With the parameters given in Table.1, the total kinetic energy K and the Kolmogorov length-

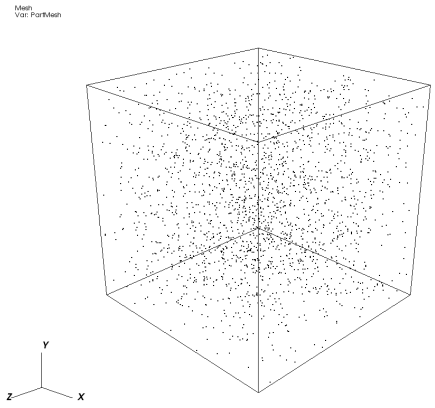

(a) Droplet distribution in the domain

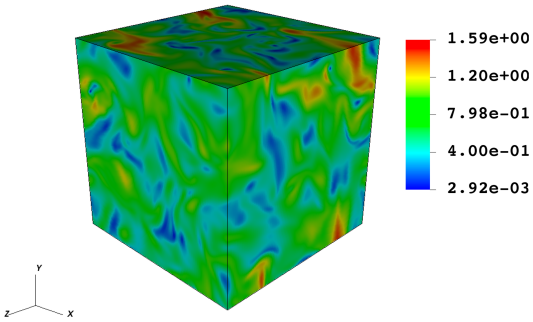

(b) Velocity magnitude (m/s) of the HIT flow

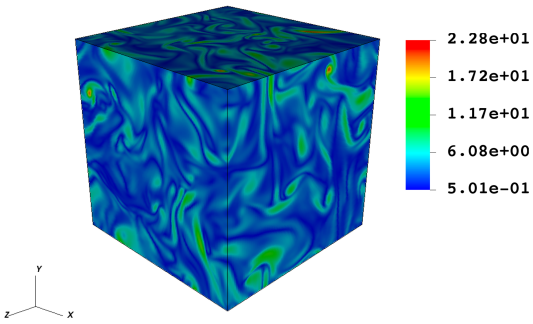

(c) Vorticity magnitude (m/s) of the HIT flow

FIGURE 1: SCHEMATIC OF THE DOMAIN

TABLE 1: PARAMETERS OF THE HIT FLOW

l (m)	ν (m^2/s)	ε (m^2/s^3)	u' (m/s)
0.0176	3.13×10^{-5}	1.40	0.411

TABLE 2: PARAMETERS OF DROPLETS

N_d	ρ_d (kg/m^3)	μ_d (kg/(m$\cdot$s))	σ (kg/s^2)	D (m)
2243	603.87	0.00020241	0.001	0.001

scale can be obtained:

$$K = \frac{1}{2}\left|u'\right|^2 = 8.46\times10^{-2}\ \mathrm{m}^2/\mathrm{s}^2 \tag{2}$$

$$\eta = \left(\nu^3/\varepsilon\right)^{1/4} = 3.85\times10^{-4}\mathrm{m} \tag{3}$$

The mesh size $\Delta x = L/N = 1.72\times10^{-4}$ m is about half of the Kolmogorov lengthscale, therefore we have a sufficient fine mesh resolution.

The physical parameters of the droplets are listed in Table.2. N_d refers to the number of droplets distributed in the flow, ρ_d is droplet density, μ_d is the dynamic viscosity, σ is droplet surface tension, and D is the diameter of droplets.

3 Methods

3.1 Flow Solver

The gas phase is solved by using an in-house code developed for direct numerical simulation (DNS) of high Reynolds number turbulent flow in a Eulerian framework [4]. The flow is governed by the Navier-Stokes equations:

$$\frac{\partial(\rho\boldsymbol{u})}{\partial t} + \nabla\cdot(\rho\boldsymbol{u}\otimes\boldsymbol{u}) = -\nabla p + \mu\nabla^2\boldsymbol{u} + \boldsymbol{f}_p^S + \boldsymbol{f}, \tag{4}$$

where $\boldsymbol{f}_p^S$ is the momentum exchange between the gas and the droplet. To prevent the decay of the turbulent kinetic energy due to dissipation, an extra forcing term $\boldsymbol{f}$ has been added to the momentum equation of the flow. The forcing term Eqn.5 is applied in physical space and is proportional to a low-pass filtered velocity field for linear forcing.

$$\boldsymbol{f} = \rho A\hat{\boldsymbol{u}} \tag{5}$$

where A is an arbitrary constant, and $\hat{\boldsymbol{u}}$ is the filtered velocity field. A is chosen such that the forcing term will make the turbulent flow to maintain its initial properties and become statistically steady. The procedure on how to determine A can be found in Ref. [4, 9].

3.2 Droplet Solver

The droplets are added to the flow with a uniform distribution in space, and their initial velocity follows the standard normal distribution. The droplets are solved by using the Larangian Particle Tracking (LPT) method. The LPT solver in our code is designed to simulate the full range of the dilute-to-dense particle laden flow [5]. Each droplet is treated as a Lagrangian particle and is governed by Eqn.6 and Eqn.7.

$$\frac{d\boldsymbol{x}_p}{dt} = \boldsymbol{u}_p \tag{6}$$

$$m_p\frac{d\boldsymbol{v}_p}{dt} = \boldsymbol{F}_p^S \tag{7}$$

In Eqn.7, $\boldsymbol{F}_p^S$ is the surface force acting on the droplet, which is the drag force in the current work. Droplet collision is not applied because the volume fraction of droplets is very small. In this study, two different droplet drag coefficient correlations has been used for the comparison between spherical and non-spherical droplet. For spherical droplets, we used PUReIBM drag law [10] given by Tenneti and Subramaniam (2011). In Tenneti and Subramaniam's work, the average fluid-particle drag is calculated by correcting the isolated droplet drag force with average viscous and pressure contributions.

$$C_d(\phi, Re_d) = \frac{C_{d,\mathrm{isol}}Re_d}{(1-\phi)^3} + F_\phi(\phi) + F_{\phi,Re_d}(\phi, Re_d) \tag{8}$$

In Eqn.8, Re_d is the droplet Reynolds number, ϕ is volume fraction of the dispersed phase. The Schiller-Naumann correlation has been used for the isolated droplet drag coefficient $C_{d,\mathrm{isol}}$. F_ϕ is the viscous correction term, and F_{ϕ,Re_d} is the pressure correction term. In the dilute limit, where ϕ is small, this correlation will reduce to the Schiller-Naumann correlation.

For non-spherical droplets, the correlation given by Helenbrook and Edwards (2002) has been adopted for the correction of droplet deformation and internal circulation [7].

$$C_d = C_{d,\mathrm{isol}}E^{-2/3}\left(\frac{2+3\mu_d/\mu}{3+3\mu_d/\mu}\right)\left(1-0.03\,(\mu/\mu_d)\,Re_d^{0.65}\right) \tag{9}$$

The aspect ratio of the deformed ellipsoidal shaped droplet E, which is defined as the ratio between the minor axis length and mojar axis length of the spheroid, is given by Eqn.10.

$$E = 1 - 0.11We^{0.82} + 0.013\sqrt{\frac{\rho_d}{\rho}}\frac{\mu}{\mu_d}Oh^{0.55}We^{1.1} \tag{10}$$

where We is the droplet Weber number defined as $We = \frac{\rho \Delta U^2 D}{\sigma}$, and Oh is the Ohnesorge number defined as $Oh = \frac{\mu_d}{\sqrt{\rho_d \sigma D}}$.

3.3 Measurement of Droplet Dispersion

Taylor's work [8] has related the problem of dispersion to the autocorrelation of Lagrangian particle velocity. In Taylor's theory, the mean square displacement of a particle within a certain time interval is proportional to the time integral of its autocorrelation. Therefore, we can use the temporal Lagrangian autocorrelation of droplet velocity as a direct measurement of droplet dispersion. The autocorrelation R_{ij} is defined in Eqn.11. The velocity with a subscription d refers to the velocity of the droplet in Lagrangian framework, and i, j refers to the direction of the velocity. The relation between the mean square displacement of a droplet in each direction $\left\langle X_{p,i}^2 \right\rangle$ and its autocorrelation is shown in Eqn.12. The Einstein summation notation is not applied in Eqn.12.

$$R_{ij}(t) = \frac{\left\langle u_{d,i}(t_0)\, u_{d,j}(t_0+t) \right\rangle}{u'_{d,i}(t_0)\, u'_{d,j}(t_0)} \tag{11}$$

$$\left\langle X_{p,i}^2 \right\rangle = 2\left\langle u_{d,i}^2 \right\rangle \int_0^t \int_0^\tau R_{ii}(\xi)\, d\xi dt \tag{12}$$

Another parameter we used for the measurement of droplet dispersion is Stokes number. In turbulent flow, due to the interaction between particles and flow structures, particles tend to accumulate in regions of high strain rate and low vorticity [11]. This phenomena is called preferential concentration, and Stokes number is one of the parameters that will affect the degree of preferential concentration. Although this measurement is indirect and qualitative, the Stokes number can also reflect the dispersion of droplets, as the more droplets are clustered, the less they are dispersed. For particles with very small Stokes number, they tend to behave like tracer particles that travel along with the streamlines of the flow; for particles with very large Stokes number, the inertia is so significant that the flow can hardly affect particles [12]. In these two cases the clustering of particles will be weaker compared to the case where particle relaxation time is comparable to flow characteristic timescale. The Stokes number is defined as the ratio between particle relaxation time $\tau_d = \frac{4\rho_d D}{3C_d \rho \Delta U}$ and the characteristic time of the flow. Depending on which timescale is used for the characteristic time of the flow, two Stokes numbers are defined. The Stokes number based on the large eddy turnover time is: $St_l = \tau_d/\tau_l$, and the Stokes number based on the Kolmogorov timescale is $St_\eta = \tau_d/\tau_\eta$. The large deddy turnove time τ_l and the Kolmogorov timescale $\tau_\eta =$ are given in Eqn.13 and Eqn.14, respectively.

$$\tau_l = \frac{l}{u'} = 4.28 \times 10^{-2}\ \text{s} \tag{13}$$

$$\tau_\eta = \sqrt{\nu/\varepsilon} = 4.73 \times 10^{-3}\ \text{s} \tag{14}$$

4 Results and Discussions

To ensure that the spheroid assumption of droplets is valid, the Weber number should be in a reasonable range such that they will not deform to irregular shape or even breakup. Our previous work [3] has shown that the drag correlation of deformed droplets will be in good accuracy when $We < 9$, while in some other literature, the Weber number for the onset of droplet breakup is around 12 [13, 14]. Therefore, in this study we first examined the Weber number of droplets to verify if they have exceeded the critical values. As can be seen in Fig.2a, the maximum droplet Weber number is initially around 5, and will decrease overtime to a value around 2, meaning the droplet will possibly have a relatively regular spheroid shape. The average Weber number decreases from 0.8 to 0.4, indicating that most droplets will not deviate too much from spherical shape.

To compare droplet dispersion of different shapes, the temporal Lagrangian autocorrelation of droplet velocity is plotted in Fig.3. The autocorrelation curves start at 1, and gradually decrease. In all directions, the non-spherical case has a higher autocorrelation compared to the spherical ones, indicating that non-spherical droplets have larger mean square displacement in the HIT flow and are better dispersed, which can be seen referring to Eqn.12.

The Stokes number of droplets also confirms this conclusion. In Fig.4, it can be found that spheroid droplets has a higher average Stokes number compared to spherical droplets, and this Stokes number is much higher than unity. Therefore, the clustering of droplets is weaker, indicating a better dispersion of non-spherical droplets.

It should be noted that, in our current simulations, the capillary time of droplet $\tau_c = \sqrt{\frac{\rho+\rho_d}{\sigma} D^3} = 2.46 \times 10^{-2}$ s. which is higher than the Kolmogorov timescale. It means that the time needed for droplet to deform and for its surface to become steady cannot be neglected, which might affect the accuracy of our results.

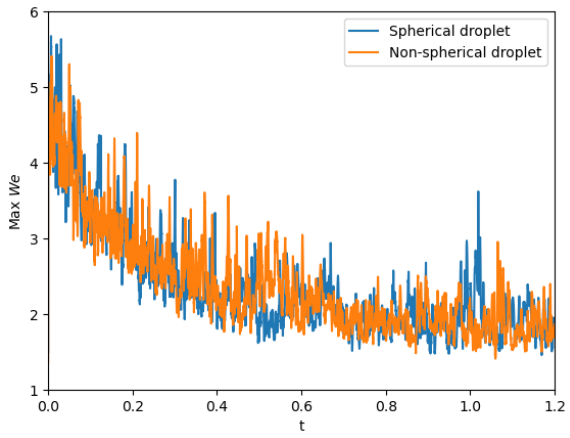

(a) Maximum Weber number of droplets

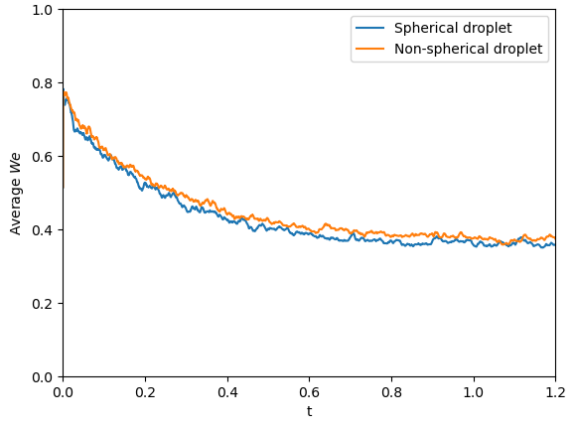

(b) Average Weber number of droplets

FIGURE 2: DROPLET WEBER NUMBER

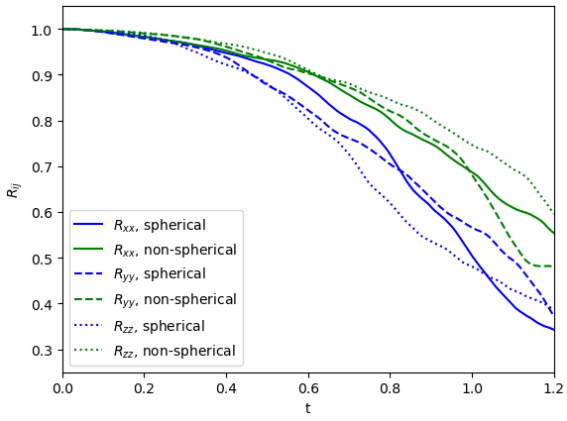

FIGURE 3: TEMPORAL LAGRANGIAN AUTOCORRELATION OF DROPLET VELOCITY

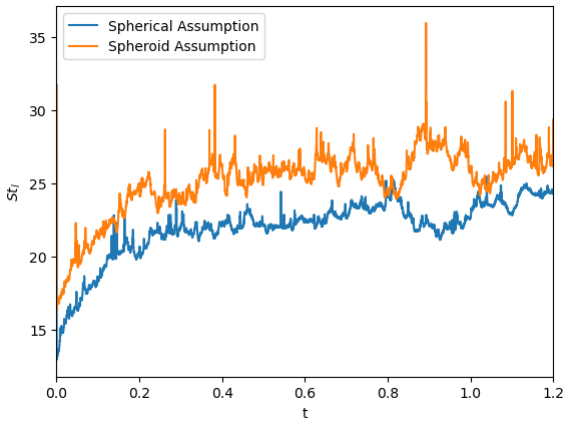

FIGURE 4: MEAN LARGE EDDY BASED STOKES NUMBER

5 Conclusions

In this study, we have compared the droplet dispersion of different shapes in homogeneous isotropic turbulent flow. The spherical and spheroidal droplets have been considered. Through numerical simulations, the HIT flow is generated by an in-house code developed for DNS of multiphase flow, and droplets are modeled by Lagrangian Particle Tracking method. The effect of droplet shape is reflected by using different drag coefficient correlations. The temporal autocorrelation of droplet velocity is used to quantify the dispersion of droplets. It has revealed that non-spherical droplets have a better dispersion in HIT flow. The mean Stokes number of droplet also confirms this result. The mean Stokes number based on large eddy timescale of spherical and non-spherical droplets are around 20, indicating that inertia effect dominates. Therefore with a larger Stokes number, the degree of preferential concentration of spherical droplets is stronger, resulting in a less dispersed status. Our current results have shown that the considering of droplet shape in modeling of spray will result in a better dispersion of droplets.

ACKNOWLEDGEMENTS

This work used ACES at the High Performance Research Computing group in Texas A&M University through allocation MCH240016 from the Advanced Cyberinfrastructure Coordination Ecosystem: Services & Support (ACCESS) program, which is supported by National Science Foundation grants #2138259, #2138286, #2138307, #2137603, and #2138296. [15]

REFERENCES

[1] Setiya, M., and Palmore, J., 2023. "Quasi-steady evaporation of deformable liquid fuel droplets". *International Journal of Multiphase Flow,* ***164***, p. 104455.

[2] Setiya, M., and Palmore Jr., J., 2023. "Combustion and Evaporation of Deformable Fuel Droplets". *ASME Journal of Heat and Mass Transfer,* ***145***(101006).
[3] Lin, Y., and Palmore Jr., J., 2022. "Effect of droplet deformation and internal circulation on drag coefficient". *Physical Review Fluids,* ***7***(12), p. 123602.
[4] Palmore Jr, J. A., and Desjardins, O., 2018. "Technique for forcing high Reynolds number isotropic turbulence in physical space". *Physical Review Fluids,* ***3***(3), Mar., pp. 1–18. Publisher: American Physical Society.
[5] Capecelatro, J., and Desjardins, O. "An euler–lagrange strategy for simulating particle-laden flows". *Journal of Computational Physics,* ***238***, pp. 1–31.
[6] O'Rourke, P. J., and Amsden, A. A., 1987. "The TAB method for numerical calculation of spray droplet breakup". In SAE Technical Papers.
[7] Helenbrook, B. T., and Edwards, C. F., 2002. "Quasi-steady deformation and drag of uncontaminated liquid drops". *International Journal of Multiphase Flow,* ***28***(10), pp. 1631–1657.
[8] Taylor, G. I., 1922. "Diffusion by continuous movements". *Proceedings of the London Mathematical Society,* ***s2-20***(1), pp. 196–212.
[9] Bassenne, M., Urzay, J., Park, G. I., and Moin, P., 2016. "Constant-energetics physical-space forcing methods for improved convergence to homogeneous-isotropic turbulence with application to particle-laden flows". *Physics of Fluids,* ***28***(3).
[10] Tenneti, S., Garg, R., and Subramaniam, S., 2011. "Drag law for monodisperse gas–solid systems using particle-resolved direct numerical simulation of flow past fixed assemblies of spheres". *International Journal of Multiphase Flow,* ***37***(9), pp. 1072–1092.
[11] Maxey, M. R., 1987. "The gravitational settling of aerosol particles in homogeneous turbulence and random flow fields". *Journal of Fluid Mechanics,* ***174***, pp. 441–465.
[12] Abrahamson, J., 1975. "Collision rates of small particles in a vigorously turbulent fluid". *Chemical Engineering Science,* ***30***(11), pp. 1371–1379.
[13] Loth, E., 2008. "Quasi-steady shape and drag of deformable bubbles and drops". *International Journal of Multiphase Flow,* ***34***(6), pp. 523–546.
[14] Hinze, J. O., 1955. "Fundamentals of the hydrodynamic mechanism of splitting in dispersion processes". *AIChE Journal,* ***1***(3), pp. 289–295.
[15] Boerner, T. J., Deems, S., Furlani, T. R., Knuth, S. L., and Towns, J., 2023. "Access: Advancing innovation: Nsf's advanced cyberinfrastructure coordination ecosystem: Services & support". In Practice and Experience in Advanced Research Computing, PEARC '23, Association for Computing Machinery, p. 173–176.